Mechanism and Kinetic Modeling for Steam Reforming of Toluene on $La_{0.8}Sr_{0.2}Ni_{0.8}Fe_{0.2}O_3$ Catalyst

Usman Oemar, Ang Ming Li, Kus Hidajat, and Sibudjing Kawi
Dept. of Chemical and Biomolecular Engineering, National University of Singapore, Singapore 117585

DOI 10.1002/aic.14573
Published online August 20, 2014 in Wiley Online Library (wileyonlinelibrary.com)

Reaction mechanism for steam reforming of toluene is proposed for $La_{0.8}Sr_{0.2}Ni_{0.8}Fe_{0.2}O_3$ perovskite catalyst. The proposed mechanism was derived from various characterization results such as temperature-programmed desorption (TPD) and temperature-programmed surface reaction (TPSR) water, TPSR toluene, TPD O_2 and in situ DRIFT of toluene decomposition, and steam reforming of toluene. Five kinetic models were developed based on the proposed dual-site reaction mechanism using Langmuir–Hinshelwood approach. Subsequently, the parameters of the kinetic models were estimated by nonlinear least square regression. A good agreement was obtained between experimental and model predicted results for the rate determining step based on reaction between adsorbed aldehyde and adsorbed oxygen. The adsorbed aldehyde species is produced from the reaction between adsorbed C_2H_2 or CH_2 and adsorbed oxygen while the adsorbed oxygen species can come from the oxygen from water activation, lattice oxygen species, and/or the redox property of some metals such as Fe. This shows that the adsorbed oxygen species plays important role in this reaction.
 AIChE J, 60: 4190–4198, 2014
Keywords: reaction mechanism, kinetic modeling, biomass tar, toluene reforming, nickel-iron, perovskite catalyst

Introduction

The use of biomass as an alternative energy for fossil fuels has been attracting vast attention recently due to the rapid depletion of fossil fuel sources and the costly price tag of crude oil. Besides production of fuels, thermochemical conversion processes are also particularly useful in harnessing heat and power with high-energy efficiencies. Among them, biomass gasification has garnered much attention for the production of synthesis gases such as hydrogen which can be used for chemical synthesis via Fischer Tropsch processes to produce methanol, dimethylether, other chemical products and electricity production in the case of a fuel cell.[1–4]

However, one of the key challenges in biomass gasification technology is the removal of tar, which is a mixture of complex condensable hydrocarbon compounds with that comprises of toluene as the major component, followed by naphthalene.[1] Tar can condense in pipe outlets and particulate filters, thereby resulting in plugging and attrition. This can lead to a decrease in efficiency of the process operations and an increase in maintenance and operating costs. Tar removal methods can be classified into physical and chemical methods of which catalytic steam reforming proves to be highly effective.

Among non-noble metals catalysts such as Ni, Co, and Fe, Ni catalyst has been used extensively in biomass gasification tar conversion, steam reforming of tar, and steam reforming of toluene as the model compound of tar as it is able to attain complete reforming of tar at temperatures of around 900°C.[5–11] In particular, it is effective in the reforming of aromatic hydrocarbons such as toluene and naphthalene that are commonly found in tar and heavy feedstock.[12] Ni catalyst also has the added advantage of catalyzing both methane reforming and water gas shift reactions thereby resulting in high H_2/CO ratio.[13] Despite its good catalytic activity in reforming reactions, Ni catalyst is susceptible to deactivation mainly through sintering of Ni^0 metallic species as well as deposition of carbon on the surface of the Ni catalyst. The agglomeration of Ni^0 particles occurs because the typical reaction temperature of 800°C is higher than its Tammann temperature (above which Ni sintering occurs).[14] Conversely, undesirable coke deposition is due to the high temperature adsorption and dissociation of tars and unsaturated hydrocarbons on the surface of the catalyst. It has been reported that coke formation can be minimized via several ways. One of them is by doping the catalyst with other metal to enhance the oxygen storage/vacancy of the catalyst.[15–17] Ashok and Kawi[18] reported that the addition of CeO_2 to the Ni/CaO-Al_2O_3 catalyst helps to reduce the carbon formation rate as compared to the unpromoted catalysts. A similar conclusion was reported by Lu et al.[19] for addition of CeO_2 to Ni/Al_2O_3 catalyst, Zhang et al.[20] for addition of CeO_2 to Ni/olivine catalyst, Soongprasit et al.[21] for substitution of Ce into $LaNiO_3$ perovskite type oxide. Bampenrat et al.[22] incorporated manganese ions to ceria lattice on Ni/CeO_2-ZrO_2 catalyst and found that the oxygen storage capacity and oxygen mobility on the catalyst surface improved, resulting in faster carbon removal. Another way is by modifying the catalyst with basic metal addition.[23–29] Viinikainen et al.[30] reported

Correspondence concerning this article should be addressed to S. Kawi at chekawis@nus.edu.sg.

Table 1. Physicochemical Properties of the LSNFO Catalysts

Catalyst	Content (mmol/g) Ni	Fe	H_2 Consumption[a] (mmol/g)	Ni-Based Reduction Degree[b] (%)	Reduced Fe Amount[c] (mmol/g)	N_2O Adsorption[d] (mmol/g)	Dispersion[e] (%)
LSNFO	3.26	0.82	3.58	111.9	0.21	0.59	16.5
LNFO	3.26	0.82	3.52	107.8	0.17	0.44	12.5

[a]H_2 consumption below 600°C in TPR profiles.[36]
[b]Stoichiometry of the Ni reduction is $Ni^{2+} + H_2 \rightarrow Ni^0 + 2H^+$.
[c]H_2 consumption > Ni content is assigned to the reduction of Fe. Stoichiometry of Fe reduction is $2Fe^{3+} + 3H_2 \rightarrow 2Fe + 6H^+$.
[d]Measured by N_2O pulse titration at room temperature.
[e]Calculated by comparing TPR-H_2 before and after N_2O pulse titration up to 600°C.

that higher basicity of catalyst can enhance the catalyst stability due to the fact that basicity is a favorable property for tar decomposition. Choong et al.[31] also reported that the addition of CaO to Ni catalyst promoted water adsorption in steam reforming of ethanol and provided abundance of adsorbed OH groups to facilitate the C—C break in Ni catalyst, resulting in higher ethanol conversion. The last option to minimize undesirable coke deposition is by operating the reaction at high reaction temperatures and excess steam-to-carbon ratio.[32]

Our previous study[33] showed that addition of Fe to Ni catalyst in perovskite type oxide enhanced the catalytic activity and stability in steam reforming of toluene due to synergistic interactions between Ni and Fe to form bimetallic Ni-Fe particles. A similar conclusion was obtained by Tomishige and coworkers[34,35] for Ni-Fe/Al_2O_3 catalyst in cellulose gasification. Furthermore, we have also shown[36] that the substitution of small amount of Sr with La in the $La_xSr_{1-x}Ni_{0.8}Fe_{0.2}O_3$ (LSNFO) perovskite catalyst delivered the good catalytic activity and stability, especially at low amount of steam (Steam/Carbon = 1) due to the inherent property of Sr in LSNFO catalyst to adsorb water strongly. Perovskite catalyst is a well-defined mixed oxide precursor catalyst with general chemical formula of ABO_3, whereby A-site is lanthanide metal (La, Ba, Ca, and Sr) and B-site is transitional metal (Ni, Co, Fe, and Cu). After full reduction, the structure will collapse and form metal on catalyst support. For LSNFO catalyst, it will form bimetallic Ni-Fe on mixed SrO-La_2O_3 catalyst support after full reduction.

To develop better catalysts, it is important to understand the possible reaction mechanism that occurs in the steam reforming of toluene. Mukai et al.[37] have performed *in situ* IR study for elucidating the reaction mechanism of toluene reforming. However, they did not propose any reaction mechanism. Duprez[38] has done extensive review on catalyst, mechanism, and kinetic model on selective toluene reforming with the objective to favor dealkylation. To the best of our knowledge, there is no literature on reaction mechanism for steam reforming of toluene to produce syngas. Hence, the objective of the present work is to propose the reaction mechanism using our LSNFO perovskite catalyst based on the characterization results and to develop the appropriate kinetic models. Identification of the correct rate determining step (RDS) is of great importance for catalyst development as the RDS is the slowest step that limits the reaction. Hence, by improving the RDS, the total reaction rate will increase.

Experimental

Catalyst synthesis

The $La_{0.8}Sr_{0.2}Ni_{0.8}Fe_{0.2}O_3$ (LSNFO) perovskite catalyst was synthesized using sol gel method using citric acid as the complexing agent as described in our previous study[33,36] and literature.[38–40] The molar ratio of Ni to Fe was 8:2, whereas the molar of Ni-Fe to La-Sr was 1:1 and the molar ratio of La-Sr to that of citric acid monohydrate was 1:2. In a typical preparation method, the required amounts of $Ni(NO_3)_2{\cdot}6H_2O$, $Fe(NO_3)_3{\cdot}9H_2O$, citric acid monohydrate, $La(NO_3)_3{\cdot}6H_2O$, and $Sr(NO_3)_2$ were dissolved in deionized water. The solution was continuously stirred at 55°C until a gel-like structure was formed. Subsequently, it was dried in an oven at 100°C overnight. The obtained xerogel precursor was calcined in a muffle furnace under air at 400°C for 30 min, followed by calcination at 850°C for 7 h. All of the chemicals used here were of analytical grade and purchased from Sigma Aldrich. The physicochemical properties of the synthesized LSNFO catalyst and the standard LNFO catalyst can be seen in Table 1.

Characterization methods

Temperature-Programmed Desorption and Temperature-Programmed Surface Reaction Measurement. The adsorption property of the catalyst was studied using temperature-programmed desorption (TPD) method. TPD of water (TPD-H_2O) for reduced catalyst were performed on the fixed-bed reactor system coupled with Thermostar Mass Spectrometer GSD 300 T. Prior to TPD-H_2O measurement, 50 mg of sample was reduced under H_2 for 1 h at 600°C, followed by cooling down under He to room temperature. The water was then introduced to the sample at room temperature for 30 mins, followed by purging under purified He gas at 100°C for 1 h. The TPD-H_2O measurement was started from 100°C to maximum temperature of 600°C under a heating rate of 10°C/min.

The decomposition of toluene and dissociation of water were studied using temperature-programmed surface reaction (TPSR) method. TPSR of water (TPSR-H_2O) and TPSR of toluene (TPSR-toluene) were also performed on a fixed-bed reactor system coupled with Thermostar Mass Spectrometer GSD 300 T. Hundred milligram of sample was pretreated at the same condition with TPD-H_2O or TPD-toluene. The toluene or water was then introduced to the sample after cooling down to room temperature using He as a carrier gas at room temperature for 30 mins, followed by ramping the furnace temperature to 800°C under a heating rate of 10°C/min.

Temperature-programmed desorption of oxygen (TPD-O_2) for reduced catalyst was also performed on Quantachrome ChemBET-3000. The sample (0.1 g) was initially reduced under H_2 for 1 h at 600°C, followed by cooling down to room temperature prior to the TPD-O_2 measurement. Purified He gas was then introduced to the system to purge out all the remaining oxygen. The TPD-O_2 measurement was started

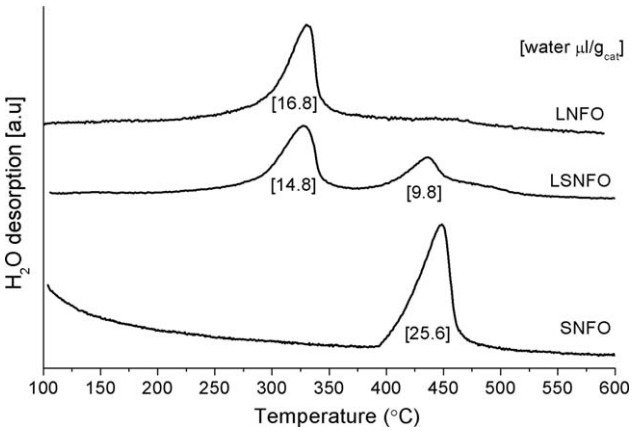

Figure 1. TPD-H_2O profiles of reduced catalysts.

from room temperature to maximum furnace temperature of 1100°C under a heating rate of 10°C/min.

In Situ DRIFT. The infrared spectra were recorded on a Bruker Vertex V70 Fourier Transform Infrared Spectrometer using the Harrick Praying Mantis DRP-4 DRIFT cell equipped with ZnSe windows and MCT detector. All spectra were collected with resolution of 4 cm^{-1} and scanned for 64 times. Prior to the analysis, the powdered sample was reduced *in situ* in H_2 gas at 600°C for 1 h. The spectra of the clean surface after reduction were recorded separately and used as a reference. Injection of 50 μL toluene for toluene decomposition or continuous flow of toluene/water mixture via bubbling was then introduced to the cell at various temperatures after 10–15 mins temperature stabilization. The spectra were then instantaneously recorded. The spectra were used after subtraction from the corresponding reference spectra.

Catalytic reaction

It is important to emphasize that in order to have reliable data for reaction kinetic, the conversion should be less than 25% for all the studied reaction conditions. Hence, the catalyst for the kinetic experiment was mixed with the inert silica in the LSNFO catalyst: quartz silica ratio of 1:9. The reactions were carried out in a quartz tube fixed bed microcatalytic reactor (ID 4 mm) enclosed in a programmable furnace at atmospheric pressure. A 50 mg of sample (5 mg of catalyst + 45 mg of quartz silica powder) held in a fixed bed using quartz wool was used for each reaction run. The inlet of the reactor was connected to a preheating coil at a temperature of 300°C to vaporize the reactants (water and toluene). A condenser at a temperature of 5°C was fitted to the outlet of the reactor to condense any unreacted water vapor and toluene vapor.

The fresh catalyst was first reduced under H_2 gas at 600°C for 1 h. Subsequently, the sample was purged by a He gas stream to remove all remaining H_2 in the system. Finally, steam and toluene were introduced into the microcatalytic reactor by liquid pumps. The steam reforming reaction is performed at various temperatures at atmospheric pressure. The amount and concentration of gaseous products were analyzed using a gas chromatograph (HP 6890 series) equipped with a packed column (Carboxen-1000, 60/80 mesh sizes) and a TCD detector. The total product volumetric flow rate was also measured using a bubble flow meter.

The chromatogram obtained for each reaction run showed peaks for H_2, CO, and CO_2 product species. The area of each peak was calculated using the integral function of the offline software coupled to the gas chromatograph. Based on the peak areas, the volume percentage of each product gases was obtained using the calibration curves that were previously determined. The individual volumetric flow rate of the product gases was obtained based on their volume percentage and the total volumetric flow rate of the product gases.

Results and Discussion

Water adsorption and activation

Figure 1 shows the TPD-H_2O measurement on reduced (LSNFO) catalyst. It can be seen that two peaks of water desorption on reduced LSNFO catalyst are observed at 230–300 and 380–500°C. To attribute the peaks correctly, the TPD-H_2O measurements were also performed on reduced catalyst without Sr ($LaNi_{0.8}Fe_{0.2}O_3$ /LNFO catalyst) and reduced catalyst without La ($SrNi_{0.8}Fe_{0.2}O_3$ /SNFO catalyst). The reduced LNFO catalyst shows one peak at lower temperature around 230–300°C, attributing to the water desorption on La_2O_3 surface, whereas reduced SNFO catalyst also shows one peak at higher temperature around 400–470°C, corresponding to water adsorption on SrO surface. The higher temperature of water desorption on SrO surface indicates that Sr has stronger binding with water than La. Hence, the peaks on reduced LSNFO catalyst can be attributed to water desorption on La_2O_3 surface for lower temperature peak (230–300°C) and water desorption on SrO surface for higher temperature peak (380–500°C). Comparing quantitative value of desorb water on reduced LSNFO catalyst revealed interesting insights. The amount of desorb water on SrO surface (9.8 μL/g_{cat}) is more than half that of the corresponding amount on La_2O_3 surface (14.8 μL/g_{cat}) even though the amount of Sr is only 20%. In addition, the total amount of desorb water on LSNFO catalyst is almost 150% compared to that on LNFO catalyst. This result shows that Sr can adsorb and desorb much more water than La.

Figure 2 shows the temperature-programmed surface reaction of water (TPSR-H_2O) on reduced LSNFO catalyst. The TPSR-H_2O result shows that H_2 production was clearly observed for LNFO and LSNFO catalysts at an onset temperature of 470°C and maximum temperature of 590°C. However, the amount of H_2 produced from LNFO catalyst

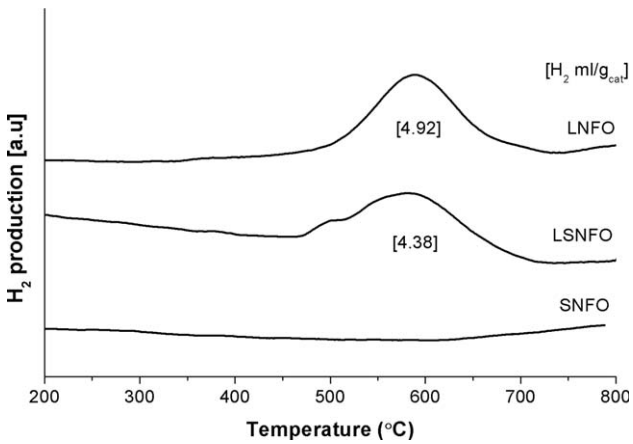

Figure 2. TPSR-H_2O profiles of reduced catalysts.

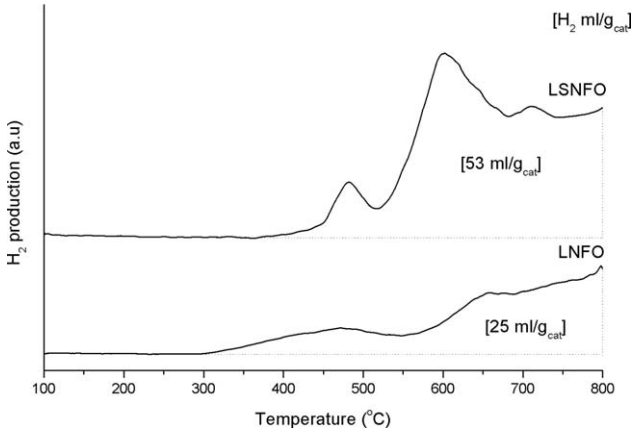

Figure 3. TPSR-toluene profile of reduced LSNFO catalyst.

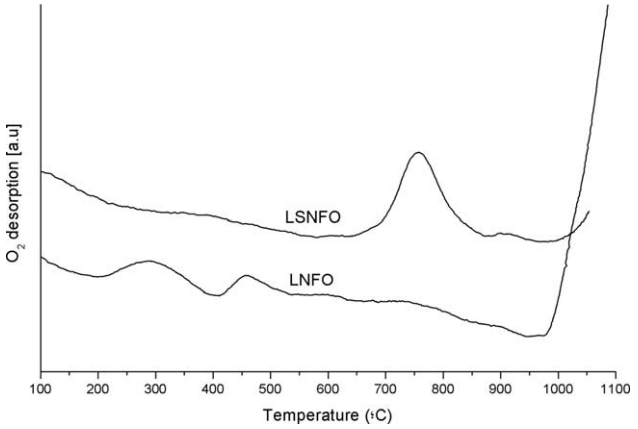

Figure 4. TPD-O_2 of reduced LSNFO catalyst.

(4.92 mL/g_{cat}) is higher than that from LSNFO catalyst (4.38 mL/g_{cat}). Conversely, there is no H_2 produced from SNFO catalyst. Our previous report[36] clearly showed that the higher H_2 production from LNFO catalyst is because LNFO catalyst contains 100% La_2O_3 which is known to be highly hygroscopic and can easily dissociate water into OH and H[41] while LSNFO catalyst contains only 80% La_2O_3. In addition, the hydrogen production due to oxygen vacancy on LSNFO catalyst should also be taken into account.

Toluene decomposition

Figure 3 shows hydrogen production from toluene decomposition on LNFO and LSNFO catalyst analyzed by mass spectrometer. As expected, toluene (C_7H_8) was decomposed mainly into hydrogen gas and deposited carbon as it only contains C and H atoms. Literature report[41,42] showed that toluene decomposition takes place via two channels: $C_6H_5CH_3 \rightarrow C_6H_5CH_2 + H$ and $C_6H_5CH_3 \rightarrow C_6H_5 + CH_3$. $C_6H_5CH_2$, C_6H_5, and CH_3 will go through further cracking to form C and H atoms which will be released as H_2 gas. The amount of H_2 production on LNFO catalyst (25 mL/g_{cat}) is smaller than the ones on LSNFO catalyst (53 mL/g_{cat}), indicating the better performance of LSNFO catalyst in toluene decomposition. The onset temperature on LSNFO catalyst is around 370°C and the maximum temperature is 610°C. Compared to the onset temperature of hydrogen production from water activation (470°C) on LSNFO catalyst discussed before, the onset temperature of toluene decomposition is located at much lower temperature, indicating that water activation is more difficult than toluene decomposition on LSNFO catalyst.

Oxygen desorption

Perovskite catalyst has been well known to possess lattice oxygen mobility due to the distortion in the molecule structure. TPD-O_2 was performed on reduced LNFO and LSNFO catalysts to see the desorption temperature of the lattice oxygen. Figure 4 shows the TPD-O_2 of reduced LNFO and LSNFO catalysts. It can be seen that LNFO catalyst shows no obvious peak but only increasing trend in intensity starting from 1000°C while LSNFO catalyst shows a peak at around 600–900°C with the maximum peak at 750°C. This peak at higher temperature can be attributed to the lattice oxygen species released from the bulk structure of the LSNFO catalyst as reported in the literature.[43,44] As the steam reforming of toluene is usually performed at temperature range of 600–800°C, this TPD-O_2 result suggests that LSNFO catalyst would have good stability for steam reforming of toluene as the lattice oxygen can help to remove carbon deposition at that temperature.

In situ DRIFT of toluene decomposition

Figure 5 shows *in situ* DRIFT spectra of toluene decomposition after 10 min of injection time on reduced LSNFO catalyst at various temperatures. At room temperature, two characteristic functional groups of toluene were obviously observed. The functional group in the range from 1300 to 1670 cm^{-1} can be attributed to the C=C stretching in the aromatic ring of toluene while the functional group at 2820–3170 cm^{-1} can be assigned to C—H stretching in the aromatic ring of toluene and methyl group.[45] These characteristic functional groups of toluene are still observed for spectra at 100 and 200°C, showing that toluene was not decomposed at these temperatures. However, these characteristic groups are no longer observed for spectra at 300°C and above, indicating that toluene had decomposed at 300°C. It is noteworthy to mention that Mukai et al.[45] have observed these two peaks for spectra at 300°C and above, attributing to the decomposition of toluene into C2 species. Derudi et al.[46]

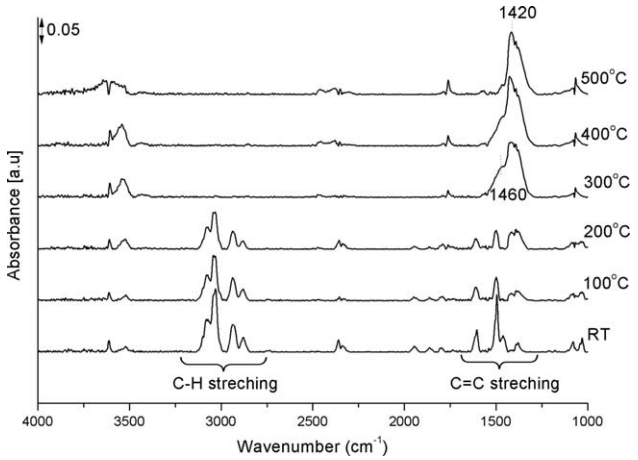

Figure 5. IR spectra of toluene decomposition at various temperatures.

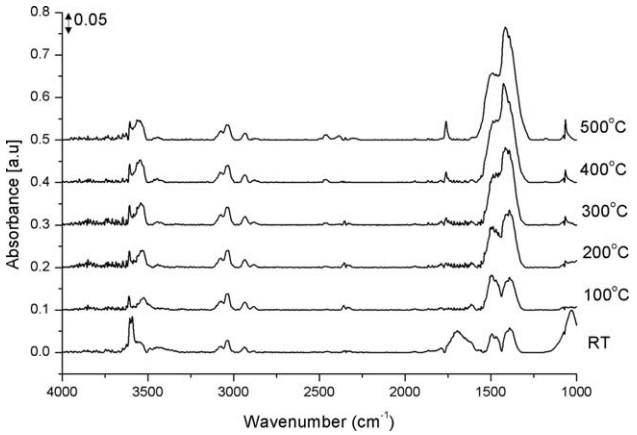

Figure 6. IR spectra of steam reforming of toluene at various temperatures.

studied the thermal decomposition of toluene at 1602 K and 1.6 bar using *ab initio* and DFT calculations and found that the final product is C_2H_2.

In situ DRIFT of steam reforming of toluene

In situ DRIFT measurement was also performed for steam reforming of toluene on reduced LSNFO catalyst. In this experiment, toluene and water were introduced continuously via bubbling to the dome cell. The measurement was taken instantaneously and the result shown in Figure 6 was recorded after 10 mins of reaction time. Figure 6 shows the presence of C—H stretching on aromatic ring of toluene and methyl group observed at 2820–3170 cm^{-1}. In addition, the functional group in the range from 3450 to 3650 cm^{-1} can be attributed to the presence of OH^- group on the catalyst. This functional group is well established for La_2O_3 supported catalyst as reported by Mu and Wang.[47] Moreover, the two peaks at wavenumber from 1280 to 1570 cm^{-1} can be attributed to the presence of C2 species which is also observed for spectra of toluene decomposition above 300°C in previous section. A more important information is derived from the peak at around 1760 cm^{-1} which can be assigned to —C═O stretching.[48] The presence of this peak combined with the presence of C—H stretching around 2820–3170 cm^{-1} shows the presence of aldehyde functional group. This result indicates the presence of aldehyde species (—CHO) on the catalyst, which can be assumed as the intermediate species.

Proposed reaction mechanism for steam reforming of toluene

Based on the above characterization results, critical information can be extracted and used to propose the reaction mechanism. First, water can dissociate on reduced LSNFO catalyst to produce H_2. The H_2 production via water can only occur via adsorption of H_2O on La_2O_3 or SrO_2 surface (Figure 1) followed by formation of adsorbed OH on La_2O_3 surface and adsorbed H. The adsorbed OH will further dissociate to adsorbed H and adsorbed O to replace the depleted oxygen on the perovskite structure. The adsorbed species of H can terminate each other to produce H_2 gas (Figure 2). Second, the toluene can decompose on the metal site of LSNFO catalyst to produce H_2 gas (Figure 3) with C2 species as the intermediate product. Specifically, toluene would adsorb on the metal site followed by the cracking of toluene into adsorbed methyl and adsorbed benzene. The adsorbed species of benzene would decompose into adsorbed species of acetaldehyde (C2 species), which was observed from *in situ* DRIFT result (Figure 5). Third, the adsorbed oxygen species (Figure 4) can react with adsorbed C2 species or adsorbed methyl species to form adsorbed aldehyde species (Figure 6). Fourth, the adsorbed aldehyde species will decompose into adsorbed CO and adsorbed hydrogen or react with adsorbed oxygen to form adsorbed CO_2. The final step is desorption step where the adsorbed CO, adsorbed CO_2, or adsorbed H_2 will desorb as CO gas, CO_2 gas, or H_2 gas, respectively. In summary, the proposed reaction mechanism can be written as follows:

1. Toluene decomposes into C2 species on metal site (s_1)

$$C_7H_8 + s_1 \overset{K_1}{\rightleftharpoons} C_7H_8 \cdot s_1 \tag{1}$$

$$C_7H_8 \cdot s_1 + s_1 \overset{K_2}{\rightleftharpoons} C_6H_6 \cdot s_1 + CH_2 \cdot s_1 \tag{2}$$

$$C_6H_6 \cdot s_1 + 2s_1 \overset{K_3}{\rightleftharpoons} 3C_2H_2 \cdot s_1 \tag{3}$$

2. Water dissociates on support site (s_2) to form H_2

$$H_2O + s_2 \overset{K_4}{\rightleftharpoons} O \cdot s_2 + H_2 \tag{4}$$

3. Reaction between active C2 species and oxygen species to form aldehyde species

$$C_2H_2 \cdot s_1 + O \cdot s_2 \overset{K_5}{\rightleftharpoons} C_2H_2O \cdot s_1 + s_2 \tag{5}$$

$$C_2H_2O \cdot s_1 + s_1 \overset{K_6}{\rightleftharpoons} CH_2O \cdot s_1 + C \cdot s_1 \tag{6}$$

$$CH_2 \cdot {}^{2s_1 + O \cdot s_2} \overset{K_7}{\rightleftharpoons} CH_2O \cdot s_1 + s_2 \tag{7}$$

$$CH_2O \cdot s_1 + s_1 \overset{K_8}{\rightleftharpoons} CHO \cdot s + H \cdot s \tag{8}$$

4. Formation of CO and CO_2 species

$$CHO \cdot s_1 + s_1 \overset{K_9}{\rightleftharpoons} CO \cdot s_1 + H \cdot s_1 \tag{9}$$

$$CO \cdot s_1 + O \cdot s_2 \overset{K_{10}}{\rightleftharpoons} CO_2 \cdot s_2 + s_1 \tag{10}$$

$$CHO \cdot s_1 + O \cdot s_2 \overset{K_{11}}{\rightleftharpoons} CO_2 \cdot s_2 + H \cdot s_1 \tag{11}$$

$$C \cdot s_1 + CO_2 \cdot s_2 \overset{K_{12}}{\rightleftharpoons} 2CO + s_1 + s_2 \tag{12}$$

5. Desorption of product species

$$CO \cdot s_1 \overset{K_{13}}{\rightleftharpoons} CO + s_1 \tag{13}$$

$$CO_2 \cdot s_2 \overset{K_{14}}{\rightleftharpoons} CO_2 + s_2 \tag{14}$$

$$2H \cdot s_1 \overset{K_{15}}{\rightleftharpoons} H_2 \cdot s_1 + s_1 \tag{15}$$

$$H_2 \cdot s_1 \overset{K_{16}}{\rightleftharpoons} H_2 + s_1 \tag{16}$$

Step (7) to step (16) are exactly the same with the elementary steps proposed by Xu and Froment[49] for steam reforming of methane taking into account reverse water gas shift reaction.

To validate the reaction mechanism and to choose the correct RDS, it is compulsory to perform kinetic study and model fitting, which will be discussed in next section.

Elimination of mass-transfer effect

Preliminary runs were performed to achieve negligible mass-transfer effects on kinetic data. The plug flow condition was used to avoid back mixing and channeling; and maintained by providing catalyst bed height to catalyst particle size ratio of $L/Dp \geq 50$ and using an internal diameter of reactor to catalyst particle size ratio of $D/Dp \geq 30$.[50] The effect of mass transfer was investigated by varying the total feed flow rates. The total volumetric feed flow rate was varied by adjusting the inert helium flow rate while the reactants (toluene and water) and products (H_2, CO, and CO_2) flow rates were kept constant. Figure 7 shows the effect of total flow rate on the catalytic activity of LSNFO catalyst. It can be seen that the toluene conversion increases with increasing total flow rate and reaches maximum at total flow rate of 490 mL/min. Above the total flow rate of 490 mL/min, the increase of toluene conversion is not significant, showing that external mass-transfer limitation does not prevail. Therefore, all the kinetic data were collected at total flow rate of 500 mL/min.

Development of kinetic models and parameter estimation

Kiennemann research group[48–52] proposed the possible reactions occuring simultaneously in steam reforming of toluene as follows

$$\text{Steam reforming } (S/C=1):\ C_7H_8+7H_2O \rightarrow 7CO+11H_2 \quad (17)$$

$$\text{Steam reforming } (S/C=2):\ C_7H_8+14H_2O \rightarrow 7CO_2+18H_2 \quad (18)$$

$$\text{Water gas shift:}\ CO+H_2O \rightleftharpoons CO_2+H_2 \quad (19)$$

$$\text{Dry reforming:}\ C_7H_8+7CO_2 \rightarrow 14CO+4H_2 \quad (20)$$

$$\text{Hydrodealkylation:}\ C_7H_8+H_2 \rightarrow C_6H_6+CH_4 \quad (21)$$

$$\text{Methane steam reforming:}\ CH_4+H_2O \rightleftharpoons CO+3H_2 \quad (22)$$

Reactions 17 and 18 represent the ideal steam reforming of toluene with *S/C* ratio of 1 and 2, respectively, while reaction 19 is water gas shift reaction which produces more H_2. The combination of reactions 17 and 19 will result in reaction 18. The produced CO_2 may react with toluene according to dry reforming of toluene (reaction 20). However, literature reports[53–55] showed that toluene conversion was quite low at 650°C for ideal dry reforming of toluene (CO_2/C_7H_8 feed ratio of 7). Hydrodealkylation (reaction 21) also possibly occurs simultaneously to produce CH_4. Produced CH_4 can then react with H_2O via steam reforming of methane (reaction 22). However, literature results[56,57] showed that presence of CH_4 in the product gases is almost negligible for all tested catalysts so far. Hence, reactions 20–22 are considered less dominant compared to reactions 17–19.

Based on the above proposed reaction mechanism, five Langmuir–Hinshelwood (LH) kinetic models were developed in this study using different RDS as follows

Model 1: Reaction 2 as RDS

$$C_7H_8 \cdot s_1+s_1 \overset{K_2}{\rightleftharpoons} C_6H_6 \cdot s_1+CH_2 \cdot s_1$$

Model 2: Reaction 3 as RDS $C_6H_6 \cdot s_1+2s_1 \overset{K_3}{\rightleftharpoons} 3C_2H_2 \cdot s_1$

Model 3: Reaction 9 as RDS $CHO \cdot s_1+s_1 \overset{K_9}{\rightleftharpoons} CO \cdot s_1+H \cdot s_1$

Model 4: Reaction 11 as RDS

$$CHO \cdot s_1+O \cdot s_2 \overset{K_{11}}{\rightleftharpoons} CO_2 \cdot s_2+H \cdot s_1$$

Model 5: Reaction 12 as RDS

$$C \cdot s_1+CO_2 \cdot s_2 \overset{K_{12}}{\rightleftharpoons} 2CO+s_1+s_2$$

The corresponding kinetic models are as follows

$$\text{Model 1: } r=\left(k_f[C_7H_8]-k_b\frac{[CO]^6[H_2]^9}{[H_2O]^6}\right)/(DEN)^2$$

$$\text{Model 2: } r=\left(k_f\frac{[C_7H_8][H_2O]}{[H_2]^2[CO]}-k_b\frac{[CO]^2[H_2]^3}{[H_2O]^2}\right)/(DEN)^2$$

$$\text{Model 3: } r=\left(k_f\frac{[C_7H_8]^{1/4}[H_2O]^{7/4}}{[H_2]^{7/4}[CO]^{3/4}}-k_b[CO][H_2]^{1/2}\right)/(DEN)^2$$

$$\text{Model 4: } r=\left(k_f\frac{[CO][H_2O]}{[H_2]^{1/2}}-k_b[CO_2][H_2]^{1/2}\right)/(DEN)^2$$

$$\text{Model 5: } r=\frac{\left(k_f\frac{[C_7H_8]^{1/3}[CO_2][H_2O]^{4/3}}{[CO]^{4/3}[H_2]^{8/3}}-k_b[CO]^2\right)}{(1+K_{CO}\cdot p_{CO}+K_{H_2}\cdot p_{H_2}+K_{toluene}\cdot p_{toluene})(1+K_{CO_2}\cdot p_{CO_2}+K_{H_2O}\cdot p_{H_2O}/p_{H_2})}$$

In developing the above models, the following assumptions were made based on observation and information well accepted in the literature:

1. The concentration of carbon-containing radicals, C_6H_6·s, CH_2·s, C_2H_2·s, CH_2O·s, CHO·s, are much lower than the total concentration of the active sites.
2. The desorption of hydrogen, CO, and CO_2 formed occur very fast.

The experimental reaction rate was expressed in terms of μmol $gcat^{-1}$ min^{-1} and calculated using plug flow reaction rate equation. The kinetic parameters were estimated based on the minimization of errors between the experimental data and the kinetic model using a combination of Gauss–Newton and Levenberg–Marquardt methods. The fitting of experimental data to the reaction rate equations was performed using MATLAB software with fmincon function. Minimization of the objective function is initiated by the random initial guesses created using Generic Algorithm method for each kinetic parameter.

To obtain all parameters value as a function of temperature, Arrhenius equation was used to obtain activation energy and pre-exponential factor according to following equation

$$k_i=A_i\exp\left[\frac{-E_i}{RT}\right]$$

Meanwhile, the equilibrium constants of the adsorbed species as a function of temperature were estimated using a Van't Hoff expression as follows

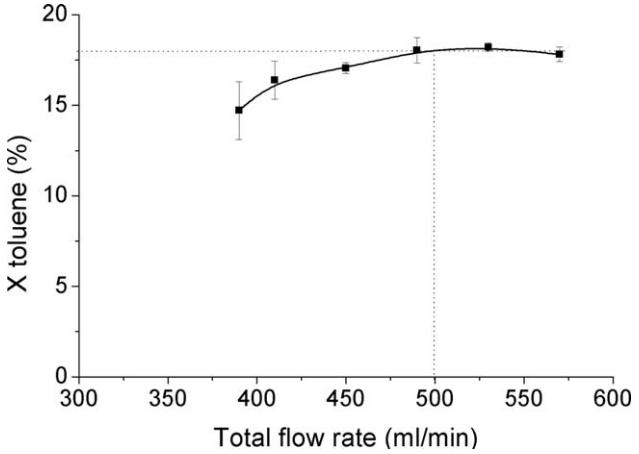

Figure 7. Effect of total flow rate on catalyst activity (Reaction condition: $T = 650^{\circ}C$, toluene 188 μmol/min; steam 1316 μmol/min; $W = 50$ mg).

$$\ln K_i = \frac{-\Delta H_i}{\mathrm{RT}} + \frac{\Delta S_i}{R}$$

The experimental conditions and results for the kinetic study are given in Table 2. The feed to the reactor contains not only the reactants (toluene and steam), but also the products (H_2, CO, and CO_2). Typically, when one of the feed flow rates is varied, the flow rate of other gases is kept constant, except for helium which is also varied to maintain the total flow rate of 500 mL/min.

The result of fitting the experimental reaction rate to the calculated reaction rate based on four models is given in Figure 8. It is found that Models 1, 2, 3, and 5 do not fit the experiment results. In contrast, Model 4 has a correlation coefficient that is near to unity ($r^2 = 0.9033$) indicating that the RDS for steam reforming of toluene is the reaction between the aldehyde species and oxygen species to produce CO_2. In addition, this model predicted an activation energy

Table 2. Experimental Conditions and Results for Kinetic Study

Reaction Temperature at 650°C						
Liquid Flow Rate (mL/min)		Gas Flow Rate (mL/min)				
Water	Toluene	CO_2	CO	H_2	He	X toluene (%)
0.05	0.04	20	50	50	Balance to	11.89
0.05	0.04	40	50	50	maintain	14.65
0.05	0.04	60	50	50	total gas	18.85
0.05	0.04	80	50	50	flow rate of	20.11
0.05	0.04	50	20	50	500 mL/min	12.92
0.05	0.04	50	40	50		14.67
0.05	0.04	50	60	50		20.58
0.05	0.04	50	80	50		25.24
0.05	0.04	50	50	20		25.63
0.05	0.04	50	50	40		22.45
0.05	0.04	50	50	60		18.50
0.05	0.04	50	50	80		15.84
0.04	0.04	50	50	50		22.34
0.05	0.04	50	50	50		21.28
0.06	0.04	50	50	50		19.21
0.07	0.04	50	50	50		18.41
0.05	0.04	50	50	50		20.59
0.05	0.05	50	50	50		14.88
0.05	0.06	50	50	50		11.80
0.05	0.08	50	50	50		8.29

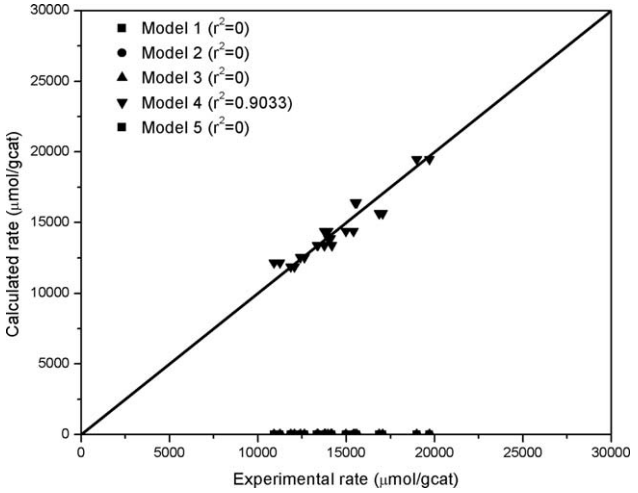

Figure 8. Parity plot of experimental and calculated reaction rate.

of 100 kJ/mol. The estimated kinetic parameters for this model is tabulated in Table 3.

Figure 9 shows the Arrhenius plot obtained by varying the reaction temperature at one reaction condition chosen from the kinetic study. The gradient of the Arrhenius plot is E_a/R obtained translates to an activation energy of 109 kJ/mol. Comparing this apparent activation energy with the predicted activation energy of Model 4, it is evident that these values are very similar. This shows that kinetic rate for steam reforming of toluene follows kinetic Model 4 which is reaction between adsorbed aldehyde species and adsorbed oxygen species. As shown in the above reaction mechanism, the adsorbed aldehyde species is produced from reaction between adsorbed C_2H_2 or CH_2 and adsorbed oxygen. The adsorbed oxygen species can be produced from oxygen from water activation, lattice oxygen species, and/or redox property of some metals such as Fe and Ce. This shows that the adsorbed oxygen species play important roles in this reaction.

Few literatures have reported the apparent activation energy for steam reforming of tar using either toluene or naphthalene as model compound. Aznar et al.[58] reported an apparent activation energy of 58 kJ/mol for tar reforming on commercial nickel catalyst. Mukai et al.[59] reported that the apparent activation energies for steam reforming of toluene are different for low temperature region and high temperature region. At low temperature region, they proposed water activation as the RDS with activation energy of 113 kJ/mol, whereas at high temperature, the RDS was proposed to be toluene decomposition with a lower activation energy of 36 kJ/mol due to the enhancement from lattice oxygen of the catalyst support. On comparison, the apparent activation energy obtained from Mukai et al. is lower than that obtained

Table 3. Estimated Kinetic Parameters for Model 4

Rate Constant	A_i (mmol/m^2 min)	E_i (kJ/mol)	ΔH_i (J/mol)	ΔS_i (J/mol K)
k_f	99	100	–	–
k_b	66	136E6	–	–
K_{CO}	–	–	−927	−71
K_{CO_2}	–	–	−875	−913
K_{H_2}	–	–	−3.7	−657
$K_{toluene}$	–	–	−151	−61
K_{H_2O}	–	–	−430	−20

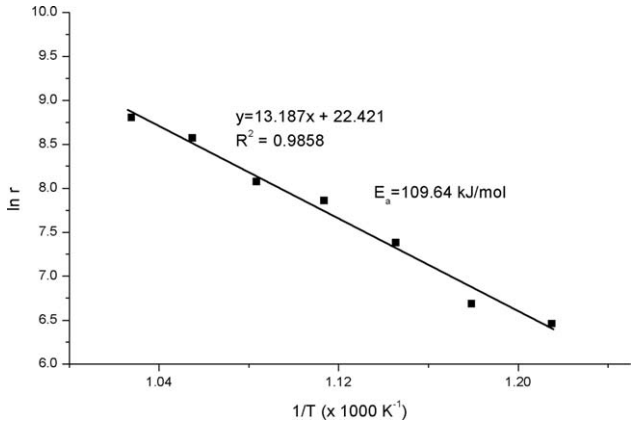

Figure 9. Arrhenius plot.

from the present study. This is probably because the present study includes product gases (H_2, CO, and CO_2) in addition to toluene and steam as the feed for the kinetic study, resulting in higher apparent activation energy. In contrast, Świerczyński et al.[60] reported high apparent activation energy of 196 kJ/mol for Ni/olivine catalyst. Similarly, Devi et al.[61] also reported activation energy of 187 kJ/mol for naphthalene reforming on pretreated olivine. Compared to these two literatures, the activation energy value derived from the present work is lower possibly because LSNFO catalyst contains lattice oxygen which can enhance the reaction as reported in literature[59] while natural olivine is comprised mainly of $(Mg_{0.94}Fe_{0.06})$-SiO_4 which does not contain lattice oxygen. However, those literatures do not provide the detail mechanism and the RDS which are of great importance for better catalyst design. Hence, the reaction mechanism and kinetic model developed in the present study can be useful for catalyst development.

Conclusions

A kinetic study for steam reforming of toluene was carried out over LSNFO perovskite catalyst over a wide range of contact times and reaction temperature in fixed bed reactor under the chemical reaction-controlled regime. The reaction mechanism was proposed based on the experiment results of TPD and TPSR water, TPSR toluene, TPD O_2 and *in situ* DRIFT of toluene decomposition, and steam reforming of toluene. The result of TPSR water of reduced LSNFO catalyst shows that water can dissociate via adsorption of H_2O on La_2O_3 or SrO surface to produce H_2. Toluene can decompose on the metal site of LSNFO catalyst to produce H_2 gas with C2 species as the intermediate product as observed from the *in situ* DRIFT result. The adsorbed oxygen species observed from TPD-O_2 can react with adsorbed C2 species or adsorbed methyl species to form adsorbed aldehyde species. The adsorbed aldehyde species will decompose into adsorbed CO and adsorbed hydrogen or react with adsorbed oxygen to form adsorbed CO_2. The final step is desorption step where the adsorbed CO, adsorbed CO_2, or adsorbed H_2 will desorb as CO gas, CO_2 gas, or H_2 gas, respectively. Five kinetic models were then developed based on the proposed reaction mechanism using LH approach. A good agreement was obtained between experimental and model predicted results for the RDS based on reaction between adsorbed aldehyde species and adsorbed oxygen species. The adsorbed aldehyde species is produced from the reaction between adsorbed C_2H_2 or CH_2 and adsorbed oxygen while the adsorbed oxygen species can come from the oxygen from water activation, lattice oxygen species, and/or the redox property of some metals such as Fe and Ce. This shows that the adsorbed oxygen species plays important role in this reaction.

Acknowledgments

The authors acknowledge financial support from National University of Singapore and NEA-ETRP (Project No. 1002 114, Research Grant No. 279-000-333-490). Usman Oemar sincerely thanks Dr. Yasotha Kathiraser, Dr. Jangam Ashok, and Mr. Saw Eng Toon for technical support and discussions.

Literature Cited

1. de Lasa H, Salaices E, Mazumder J, Lucky R. Catalytic steam gasification of biomass: catalysts, thermodynamics and kinetics. *Chem Rev*. 2011;111:5404–5433.
2. Buchireddy PR, Bricka RM, Rodriguez J, Holmes W. Biomass gasification: catalytic removal of tars over zeolites and nickel supported zeolites. *Energy Fuel*. 2010;24:2707–2715.
3. Han J, Kim H. The reduction and control technology of tar during biomass gasification/pyrolysis: an overview. *Renew Sustain Energy Rev*. 2008;12:397–416.
4. Huber GW, Iborra S, Corma A. Synthesis of transportation fuels from biomass: chemistry, catalysts, and engineering. *Chem Rev*. 2006;106:4044–4098.
5. Sombatsompop N, Bhattacharyya D, Cheung KH-Y. Bimetallic $LaNi_{1-x}Co_xO_3$ (x = 0, 0.3, 0.5, 0.7, and 1) perovskite catalysts for tar reforming to syngas. *Adv Mater Res*. 2013;747:690–693.
6. Wu C, Williams PT. Nickel-based catalysts for tar reduction in biomass gasification. *Biofuels*. 2011;2:451–464.
7. Nishikawa J, Miyazawa T, Nakamura K, Asadullah M, Kunimori K, Tomishige K. Promoting effect of Pt addition to $Ni/CeO_2/Al_2O_3$ catalyst for steam gasification of biomass. *Catal Commun*. 2008;9:195–201.
8. Kimura T, Miyazawa T, Nishikawa J, Kado S, Okumura K, Miyao T, Naito S, Kunimori K, Tomishige K. Development of Ni catalysts for tar removal by steam gasification of biomass. *Appl Catal B*. 2006;68:160–170.
9. El-Rub ZA, Bramer EA, Brem G. Review of catalysts for tar elimination in biomass gasification processes. *Ind Eng Chem Res*. 2004; 43:6911–6919.
10. Coll R, Salvadó J, Farriol X, Montané D. Steam reforming model compounds of biomass gasification tars: conversion at different operating conditions and tendency towards coke formation. *Fuel Process Technol*. 2001;74:19–31.
11. Guana G, Chen G, Kasai Y, Lim EWC, Hao X, Kaewpanha M, Abuliti A, Fushimi C, Tsutsumi A. Catalytic steam reforming of biomass tar over iron- or nickel-based catalyst supported on calcined scallop shell. *Appl Catal B*. 2012;115–116:159–168.
12. Bangala DN, Abatzoglou N, Chornet E. Steam reforming of naphthalene on $Ni\text{-}Cr/Al_2O_3$ catalysts doped with MgO, TiO_2 and La_2O_3. *AIChE J*. 1998;44:927–936.
13. Zhao B, Zhang X, Chen L, Qu R, Meng G, Yi X, Sun L. Steam reforming of toluene as model compound of biomass pyrolysis tar for hydrogen. *Biomass Bioenergy*. 2010;34:140–144.
14. Trimm DL. Catalysts for the control of coking during steam reforming. *Catal Today*. 1999;49:3–10.
15. Koike M, Ishikawa C, Li D, Wang L, Nakagawa Y, Tomishige K. Catalytic performance of manganese-promoted nickel catalysts for the steam reforming of tar from biomass pyrolysis to synthesis gas. *Fuel*. 2013;103:122–129.
16. Li C, Hirabayashi D, Suzuki K. A crucial role of O_2^- and O_{22}^- on mayenite structure for biomass tar steam reforming over $Ni/Ca_{12}Al_{14}O_{33}$. *Appl Catal B*. 2009;88:351–360.
17. Nishikawa J, Nakamura K, Asadullah M, Miyazawa T, Kunimori K, Tomishige K. Catalytic performance of $Ni/CeO_2/Al_2O_3$ modified with noble metals in steam gasification of biomass. *Catal Today*. 2008;131:146–155.
18. Ashok J, Kawi S. Steam reforming of toluene as a biomass tar model compound over CeO_2 promoted $Ni/CaO\text{–}Al_2O_3$ catalytic systems. *Int J Hydrogen Energy*. 2013;38:13938–13949.
19. Lu Y, Li S, Guo L, Zhang X. Hydrogen production by biomass gasification in supercritical water over $Ni/\gamma Al_2O_3$ and $Ni/CeO_2\text{-}\gamma Al_2O_3$ catalysts. *Int J Hydrogen Energy*. 2010;35:7161–7168.

20. Zhang R, Wang Y, Brown RC. Steam reforming of tar compounds over Ni/olivine catalysts doped with CeO_2. *Energy Convers Manag*. 2007;48:68–77.
21. Soongprasit K, Aht-Ong D, Sricharoenchaikul V, Atong D. Synthesis and catalytic activity of sol-gel derived La–Ce–Ni perovskite mixed oxide on steam reforming of toluene. *Curr Appl Phys*. 2012;12:S80–S88.
22. Bampenrat A, Meeyoo V, Kitiyanan B, Rangsunvigit P, Rirksomboon T. Naphthalene steam reforming over Mn-doped CeO_2–ZrO_2 supported nickel catalysts. *Appl Catal A*. 2010;373:154–159.
23. Zamboni I, Courson C, Niznansky D, Kiennemann A. Simultaneous catalytic H_2 production and CO_2 capture in steam reforming of toluene as tar model compound from biomass gasification. *Appl Catal B*. 2013;145:63–72.
24. Bimbela F, Chen D, Ruiz J, Garcia L, Arauzo J. Ni/Al coprecipitated catalysts modified with magnesium and copper for the catalytic steam reforming of model compounds from biomass pyrolysis liquids. *Appl Catal B*. 2012;119–120:1–12.
25. Li D, Wang L, Koike M, Nakagawa Y, Tomishige K. Steam reforming of tar from pyrolysis of biomass over Ni/Mg/Al catalysts prepared from hydrotalcite-like precursors. *Appl Catal B*. 2011;102:528–538.
26. Carrero A, Calles JA, Vizcaino AJ. Effect of Mg and Ca addition on coke deposition over Cu-Ni/SiO_2 catalysts for ethanol steam reforming. *Chem Eng J*. 2010;163:395–402.
27. Nakamura K, Miyazawa T, Sakurai T, Miyao T, Naito S, Begum N, Kunimori K, Tomishige K. Promoting effect of MgO addition to Pt/Ni/CeO_2/Al_2O_3 in the steam gasification of biomass. *Appl Catal B*. 2009;86:36–44.
28. Lisboa JS, Santos DCRM, Passos FB, Noronha FB. Influence of the addition of promoters to steam reforming catalysts. *Catal Today*. 2005;101:15–21.
29. Świerczyński D, Libs S, Courson C, Kiennemann A. Steam reforming of tar from a biomass gasification process over Ni/olivine catalyst using toluene as a model compound. *Appl Catal B*. 2007;74:211–222.
30. Viinikainen T, Rönkkönen H, Bradshaw H, Stephenson H, Airaksinen S, Reinikainen M, Simell P, Krause O. Acidic and basic surface sites of zirconia-based biomass gasification gas clean-up catalysts. *Appl Catal A*. 2009;362:169–177.
31. Choong CKS, Huang L, Zhong Z, Lin J, Hong L, Chen L. Effect of calcium addition on catalytic ethanol steam reforming of Ni/Al_2O_3: acidity/basicity, water adsorption and catalytic activity. *Appl Catal A*. 2011;407:155–162.
32. Świerczyński D, Courson C, Kiennemann A. Study of steam reforming of toluene used as model compound of tar produced by biomass gasification. *Chem Eng Process*. 2008;47:508–513.
33. Oemar U, Ang PS, Hidajat K, Kawi S. Promotional effect of Fe on perovskite $LaNi_xFe_{1-x}O_3$ catalyst for hydrogen production via steam reforming of toluene. *Int J Hydrogen Energy*. 2013;38;5525–5534.
34. Wang L, Li D, Koike M, Koso S, Nakagawa Y, Xu Y, Tomishige K. Catalytic performance and characterization of Ni-Fe catalysts for the steam reforming of tar from biomass pyrolysis to synthesis gas. *Appl Catal A*. 2011;392:248–255.
35. Koike M, Li D, Nakagawa Y, Tomishige K. A highly active and coke-resistant steam reforming catalyst comprising uniform nickel–iron alloy nanoparticles. *ChemSusChem*. 2012;5:2312–2314.
36. Oemar U, Ang ML, Hee WF, Hidajat K, Kawi S. Perovskite LaxM1-xNi0.8Fe0.2O3 catalyst for steam reforming of tar: crucial role of alkali earth metal at low steam condition. *Appl Catal B*. 2014;148–149:231–242.
37. Mukai D, Murai Y, Higo T, Tochiya S, Hashimoto T, Sugiura Y, Sekine Y. In situ IR study for elucidating reaction mechanism of toluene steam reforming over Ni/$La_{0.7}Sr_{0.3}AlO_{3-\delta}$ catalyst. *Appl Catal A*. 2013;466:190–197.
38. Duprez D. Selective steam reforming of aromatic compounds on metal catalyst. *Appl Catal A*. 1992;82:111–157.
39. Maneerung T, Hidajat K, Kawi S. $LaNiO_3$ perovskite catalyst precursor for rapid decomposition of methane: influence of temperature and presence of H_2 in feed stream. *Catal Today*. 2011;171:24–35.
40. Sutthiumporn K, Maneerung T, Kathiraser Y, Kawi S. CO_2 dry-reforming of methane over $La_{0.8}Sr_{0.2}Ni_{0.8}M_{0.2}O_3$ perovskite (M = Bi, Co, Cr, Cu, Fe): roles of lattice oxygen on C–H activation and carbon suppression. *Int J Hydrogen Energy*. 2012;37:11195–11207.
41. Kwon J, Dai M, Halls MD, Langereis E, Chabal YJ, Gordon RG. In situ infrared characterization during atomic layer deposition of lanthanum oxide. *J Phys Chem C*. 2009;113:654–660.
42. Oehlschlaeger MA, Davidson DF, Hanson RK. Thermal decomposition of toluene: overall rate and branching ratio. *Proc Combust Inst*. 2007;1:211–219.
43. Oemar U, Hidajat K, Kawi S. Role of catalyst support over PdO–NiO catalysts on catalyst activity and stability for oxy-CO_2 reforming of methane. *Appl Catal A*. 2011;402:176–187.
44. Kaliaguine S, Van Neste A, Szabo V, Gallot JE, Bassir M, Muzychuk R. Perovskite-type oxides synthesized by reactive grinding: part I. *Preparation and characterization*. *Appl Catal A*. 2001;209:345–358.
45. Mukai D, Murai Y, Higo T, Tochiya S, Hashimoto T, Sugiura Y, Sekine Y. In situ IR study for elucidating reaction mechanism of toluene steam reforming over Ni/$La_{0.7}Sr_{0.3}AlO_{3-\delta}$ catalyst. *Appl Catal A*. 2013;466:190–197.
46. Derudi M, Polino D, Cavallotti C. Toluene and benzyl decomposition mechanisms: elementary reactions and kinetic simulations. *Phys Chem Chem Phys*. 2011;13:21308–21318.
47. Mu Q, Wang Y. Synthesis, characterization, shape-preserved transformation, and optical properties of $La(OH)_3$, $La_2O_2CO_3$, and La_2O_3 nanorods. *J Alloy Compd*. 2011;509:396–401.
48. Topalian Z, Stefanov BI, Granqvist CG, Österlund L. Adsorption and photo-oxidation of acetaldehyde on TiO_2 and sulfate modified TiO_2: studies by in situ FTIR spectroscopy and micro-kinetic modeling. *J Catal*. 2013;307:265–274.
49. Xu J, Froment GF. Methane steam reforming, methanation and water-gas shift: I. *Intrinsic kinetics*. *AIChE J*. 1989;35:88–96.
50. Froment GF, Bischoff KB. *Chemical Reactor Analysis and Design*, 2nd ed. New York: Wiley, 1990.
51. Felice LD, Courson C, Foscolo PU, Kiennemann A. Iron and nickel doped alkaline-earth catalysts for biomass gasification with simultaneous tar reformation and CO_2 capture. *Int J Hydrogen Energy*. 2011;36:5296–5310.
52. Rapagná S, Provendier H, Petit C, Kiennemann A, Foscolo PU. Development of catalysts suitable for hydrogen or syn-gas production from biomass gasification. *Biomass Bioenergy*. 2002;22:377–388.
53. Chen T, Liu H, Shi P, Chen D, Song L, He H, Frost RL. CO_2 reforming of toluene as model compound of biomass tar on Ni/Palygorskite. *Fuel*. 2013;107:699–705.
54. Kong M, Yang Q, Fei J, Zheng X. Experimental study of Ni/MgO catalyst in carbon dioxide reforming of toluene, a model compound of tar from biomass gasification. *Int J Hydrogen Energy*. 2012;37:13355–13364.
55. Kong M, Fei J, Wang S, Lu W, Zheng X. Influence of supports on catalytic behavior of nickel catalysts in carbon dioxide reforming of toluene as a model compound of tar from biomass gasification. *Bioresour Technol*. 2011;102:2004–2008.
56. Koike M, Hisada Y, Wang L, Li D, Watanabe H, Nakagawa Y, Tomishige K. High catalytic activity of Co-Fe/α-Al_2O_3 in the steam reforming of toluene in the presence of hydrogen. *Appl Catal B*. 2013;140–141:652–662.
57. Sekine Y, Mukai D, Murai Y, Tochiya S, Izutsu Y, Sekiguchi K, Hosomura N, Arai H, Kikuchi E, Sugiura Y. Steam reforming of toluene over perovskite-supported Ni catalysts. *Appl Catal A*. 2013;451:160–167.
58. Aznar MP, Caballero MA, Gil J, Martin JA, Corella J. Commercial steam reforming catalysts to improve biomass gasification with steam−oxygen mixtures. 2. Catalytic tar removal. *Ind Eng Chem Res*. 1998;37:2668–2680.
59. Mukai D, Tochiya S, Murai Y, Imori M, Sugiura Y, Sekine Y. Structure and activity of Ni/$La_{0.7}Sr_{0.3}AlO_{3-\delta}$ catalyst for hydrogen production by steam reforming of toluene. *Appl Catal A*. 2013;464–465:78–86.
60. Świerczyński D, Libs S, Courson C, Kiennemann A. Steam reforming of tar from a biomass gasification process over Ni/olivine catalyst using toluene as a model compound. *Appl Catal B*. 2007;74:211–222.
61. Devi L, Ptasinski KJ, Janssen FJJG. Pretreated olivine as tar removal catalyst for biomass gasifiers: investigation using naphthalene as model biomass tar. *Fuel Process Technol*. 2005;86:707–730.

Manuscript received Mar. 13, 2014, and revision received July 15, 2014.